Title

Improving Quantitative Accuracy in Nontargeted Lipidomics by Evaluating Adduct Formation.

Journal

Analytical Chemistry, 95(34)

Authors

Bishop, Lauren

Shen, Tong

Fiehn, Oliver

Publication Date

2023-08-29

DOI

10.1021/acs.analchem.3c01221

Peer reviewed

HHS Public Access

Author manuscript

Anal Chem. Author manuscript; available in PMC 2024 December 13.

Published in final edited form as:

Anal Chem. 2023 August 29; 95(34): 12683–12690. doi:10.1021/acs.analchem.3c01221.

Improving Quantitative Accuracy in Nontargeted Lipidomics by Evaluating Adduct Formation

Lauren M. Bishop,
Department of Chemistry, University of California Davis, Davis, California 95616, United States

Tong Shen,
West Coast Metabolomics Center, 451 Health Sci. Drive, University of California Davis, Davis, California 95616, United States

Oliver Fiehn
West Coast Metabolomics Center, 451 Health Sci. Drive, University of California Davis, Davis, California 95616, United States

Abstract

For large-scale lipidomic analyses, accurate and reproducible quantification of endogenous lipids is crucial for comparing results within and across studies. Many lipids present in liquid chromatography–electrospray ionization–mass spectrometry form various adducts with buffer components. The mechanisms and conditions that dictate adduct formation are still poorly understood. In a positive mode, neutral lipids like mono-, di-, and triacylglycerides and cholesteryl esters typically generate $[M + NH_4]^+$ adduct ions, although $[M + Na]^+$, $[M + K]^+$, and other (more complex) species can also be significantly abundant in MS1 precursor ion spectra. Variations in the ratios of these adducts (within and between matrices) can lead to dramatic inaccuracies during quantification. Here, we examine 48 unique diacylglycerol (DAG) species across 2366 mouse samples for eight matrix-specific data sets of plasma, liver, kidney, brain, heart muscle, gastrocnemius muscle, gonadal, and inguinal fat. Typically, no single adduct ion species accounted for more than 60% of the total observed abundance across each data set. Even within a single matrix, DAGs showed a high variability of adduct ratios. The ratio of $[M + NH_4]^+$ adduct ions was increased for longer-chain DAGs and for polyunsaturated DAGs, at the expense of reduced ratios of $[M + Na]^+$ adducts. When using three deuterated internal DAG standards, we found that absolute concentrations were estimated with up to 70% error when only one adduct ion was used instead of all adducts combined. Importantly, when combining $[M + NH_4]^+$ and $[M + Na]^+$ adduct ions, quantification results were within 5% accuracy compared to all adduct ions

Corresponding Author: Oliver Fiehn – West Coast Metabolomics Center, 451 Health Sci. Drive, University of California Davis, Davis, California 95616, United States; ofiehn@ucdavis.edu.

Author Contributions

L.M.B., T.S., and O.F. conceived the study. L.M.B. performed data analysis and produced figures and tables. L.M.B. and O.F. wrote the manuscript. O.F. supervised the research. All authors reviewed and edited the manuscript.

Supporting Information

The Supporting Information is available free of charge at https://pubs.acs.org/doi/10.1021/acs.analchem.3c01221.

Average adduct ratios for all lipids in all matrices and variance attributed to combining adduct forms (PDF)

Comparison of matrix-specific trends in adduct formation according to carbon chain length and degree of unsaturation (XLSX)

Complete contact information is available at: https://pubs.acs.org/10.1021/acs.analchem.3c01221

The authors declare no competing financial interest.

combined. Additional variance can be caused by other factors, such as instrument conditions or matrix effects.

Graphical Abstract

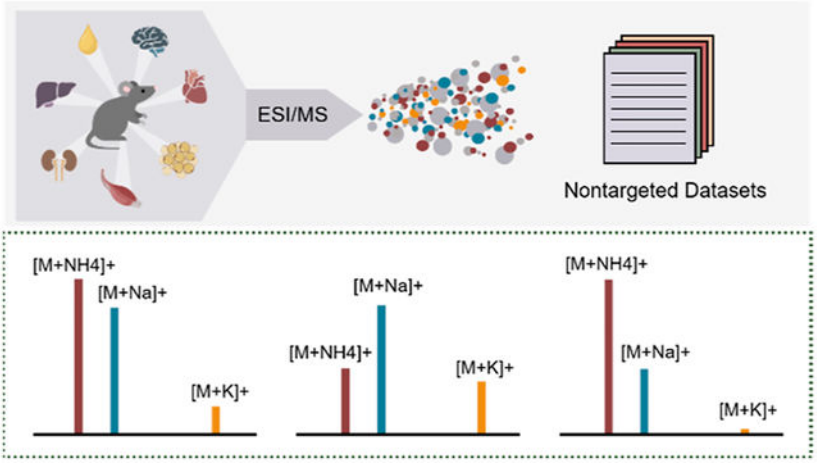

INTRODUCTION

The ability to identify hundreds of endogenous lipids using nontargeted workflows has made lipidomic analysis an important tool for biological discoveries. As methods for comprehensive lipid profiling have become more robust by liquid chromatography–high-resolution tandem mass spectrometry (LC–HRMS/MS), the complexity and scale of these analyses have continued to increase. In response to the upsurge of large-scale analyses, recent studies have explored the reliability of these methods through assessment of batch effects, differences in LC–MS platforms, and interlab performances.[1–3] Despite continuous advancements in LC–MS, nontargeted workflows remain challenged by issues of repeatability, data transferability, and quantitative accuracy.[4,5]

For both targeted and nontargeted analyses, it is most common to use the most abundant adduct form to represent an entire lipid subclass. Yet, LC–MS1 data are composed of thousands of *m*/*z*-retention time features that include natural isotopes, in-source fragments, and adducts. While these features are typically low abundant and often removed from analysis, adduct ions are regularly utilized for reporting the (semi)quantitative abundances of lipids.[6,7] In nontargeted lipidomic analyses by positive mode electrospray ionization (+ESI), polar lipid species will often yield protonated ion types $[M + H]^+$, whereas neutral lipids will primarily form ammoniated $[M + NH_4]^+$ and sodiated $[M + Na]^+$ adducts.[8] However, many lipid subclasses can also form abundant adduct species with alkali metals or experience in-source neutral losses, such as $[M + H - H_2O]^+$.[9,10] This variability in adduct formation is caused by both technical and biological factors. LC mobile phase additives, system contaminants, and matrix components are known to alter adduct ratios.[11,12] Previous studies have proposed methods to reduce or enhance specific adducts,[13,14] but such alterations may not be suitable to measure hundreds of lipids across many lipid classes. Even data interpretation may be altered when different adduct forms are selected.[15] Strangely, links

between adduct selection and quantitative accuracy have not been thoroughly investigated yet, although tools such as MS-FLO, CAMERA, RAMClustR, and Binner currently assist in identifying and joining adduct species.[16–19]

Hence, we explore the extent of variability in adduct formation in nontargeted lipidomic analyses and its impact on the quantitative accuracy. To evaluate adduct trends, eight data sets of different tissue matrices acquired between two instruments were analyzed for ESI positive mode adduct forms. For this analysis, diacylglycerol (DAG) species were utilized to demonstrate trends in adduct formation, given their proclivity for forming multiple significantly abundant adducts. Potential contributing factors to adduct ratio variability were investigated such as peak intensity, acyl group length, degree of unsaturation, and the biological matrix. Additionally, we compare the use of single adducts to joining adducts on the impacts of both relative quantification and absolute quantification via the estimation of molar concentrations. Resulting from this work, guidelines for proper adduct selection are proposed.

EXPERIMENTAL SECTION

Materials.

UltimateSPLASH ONE lipidomics standards and supplemental standards of oleic acid-D9, arachidonic acid-D11, cholesterol-D7, and C17-sphingosine were purchased from Avanti Polar Lipids. Additional supplement standards of decanoyl-L-carnitine-D3, dodecanoyl-L-carnitine-D3, and octadecanoyl-L-carnitine-D3 were purchased from Cambridge Isotope Laboratories, and palmitic acid-D3 was purchased from CDN Isotopes. All reagents used were of LC–MS grade. Biological samples were provided as part of the mouse longevity project of the NIH Longevity Consortium. Mice were procured and maintained as previously described.[20] Tissue samples of gonadal fat, inguinal fat, gastrocnemius muscle (gastroc), liver, kidney, heart, brain, and blood plasma were harvested and stored at −80 °C until analysis.

Sample Preparation.

Gastrocnemius muscle, liver, kidney, heart, and brain samples were lyophilized for 24 h and homogenized using a SPEX SamplePrep 2010 GenoGrinder prior to extraction. The gonadal fat and inguinal fat samples were homogenized using a SPEX SamplePrep 2010 GenoGrinder concomitant with extractions. Twenty μL of plasma, 5 mg of gonadal and inguinal fat, 2 mg of lyophilized gastrocnemius muscle, and 1 mg of lyophilized liver, kidney, heart, and brain tissue samples were extracted by suspending in 225 μL of −20 °C cold methanol treated with the UltimateSPLASH ONE and supplemental standards. 750 μL of −20 °C cold methyl-*tert*-butyl ether (MTBE) containing a cholesteryl ester 22:1 standard was added to each sample and then vortexed for 10 min. Next, 188 μL of LC–MS grade water was added and vortexed for 5 min to induce the phase separation. Samples were centrifuged for 2 min at 14,000*g* before 350 μL of the upper nonpolar layer was collected and dried. 175 μL of the nonpolar phase was dried for the gonadal fat and inguinal fat samples due to the high lipid content of the matrix type. The remaining fractions of matrix-containing samples were combined to form pooled quality control (QC) samples.

Samples were resuspended using 100 μL of methanol/toluene (9:1, v/v) with 50 ng/mL of 12-[(cyclohexylamine) carbonyl]amino]-dodecanoic acid (CUDA) and stored at −20 °C until analysis.

LC–MS/MS Data Acquisition.

For nontargeted lipidomics analysis, 1 μL (gonadal and inguinal fat), 2 μL (gastroc), and 3 μL (plasma, liver, kidney, heart, and brain) of the resuspended nonpolar phase was injected into two Thermo-Fisher Scientific Vanquish UHPLC + liquid chromatography systems coupled to Q-Exactive HF orbital ion trap mass spectrometers. The LC system was equipped with a Waters Acquity UPLC CSH C18 column (100 × 2.1 mm; 1.7 μm) and a Waters Acquity VanGuard CSH C18 precolumn (5 × 2.1 mm; 1.7 μm). The column compartment and mobile phase preheater were set at 65 °C, and the mobile phase flow rate was 0.6 mL/min. Mobile phase A was acetonitrile/water (60/40, v/v) with 0.1% formic acid and 10 mM ammonium formate as modifiers, and mobile phase B consisted of isopropanol/acetonitrile (90:10, v/v) with 0.1% formic acid and 10 mM ammonium formate. The LC gradient started with mobile phase B at 15%, increasing to 30% between 0 and 2 min. B was brought from 30 to 48% between 2 and 2.5 min, 48 to 82% between 2.5 and 11 min, and 82 to 99% from 11 to 11.5 min 99% B was maintained between 11.5 and 12 min and then brought back to 15% between 12 and 12.1 min and held there between 12.1 and 14.2 min for re-equilibration. The injection needle was washed 10 s after each injection with isopropanol.

Positive mode electrospray ionization (ESI+) used a spray voltage of 3.6 kV, capillary temperature of 300C, sheath gas flow rate of 60 units nitrogen, and auxiliary gas flow rate of 25 units nitrogen. Data were collected from 0 to 13 min of the LC gradient in the scan range of 120–1700 m/z using data-dependent acquisition (DDA) with the top four ions from each MS1 scan being selected for MS/MS fragmentation. DDA MS/MS was acquired with a stepped normalized collision energy of 20, 30, and 40%. MS1 spectra were collected with a resolving power setting of 60,000 measured at 200 m/z, and MS/MS spectra were collected at a resolving power setting of 15,000. To increase the total number of MS/MS spectra, five consecutive runs were made using the R package “IE-Omics”[21] for each matrix type under positive electrospray conditions. All spectra were stored in centroid, “.raw” format.

Data Analysis and Adduct Selection.

The data were converted from “.raw” format into “.abf” format using the Analysis Base File converter. Deconvolution, peak picking, alignment, and compound identification were completed through open source software MS-DIAL v4.48.[22] Compounds were annotated using an internally curated mzRT library where lipids were matched by accurate mass and retention time, as well as matching accurate precursor masses and MS/MS fragmentation patterns against the LipidBlast library.[23] Annotated DAG species were isolated from each completed data set and reprocessed through MS-FLO to identify ion adducts, duplicate peaks, and isotopic features.[16] $[M + NH_4]^+$, $[M + Na]^+$, $[M + K]^+$, $[M + H - H_2O]^+$, $[M + H]^+$, and dimerized adduct forms were considered. All adduct ions were verified by accurate mass, retention time, and correlations of peak intensity between adduct types of the same DAG compound. Peak height was used as the spectral intensity for all data analysis. Samples were normalized by Systematic Error Removal by Random Forest (SERRF)[24] to correct

for instrument signal drifts. Protonated and dimerized DAG species were detected when the lipid was highly abundant but were consistently measured at 1–2% of the total abundance. These adduct forms were never consistently measured above 5% for the eight matrices analyzed; therefore, they were omitted from analysis. Three deuterated, monounsaturated DAG standards of known concentrations were included in the acquisition and utilized for estimations of absolute molar concentrations.

RESULTS AND DISCUSSION

We identified 48 unique DAG species across eight mouse matrices: blood plasma (Pl), gonadal fat (GF), inguinal fat (IF), gastrocnemius muscle (gastroc, Gs), liver (Lv), kidney (Kd), heart (Ht), and brain (Br). All deuterated DAG internal standards were measured in all samples. Through evaluation of all matrices, four adduct species were found to be the most common; $[M + Na]^+$, $[M + NH_4]^+$, $[M + K]^+$, and $[M + H - H_2O]^+$. Protonated and dimerized adduct forms were consistently absent or low abundant in the data sets and omitted from this analysis. Adduct response ratios for each DAG molecule were calculated from the summed intensities of the four adducts measured in this analysis.

Evaluation of Adduct Ratios.

To explore the impact of adduct formation on large-scale lipidomics studies, we analyzed the differences in adduct ratios from three perspectives: across individual biological samples, between different DAG species, and between data sets of different tissue matrices. Utilizing results from more than 240 unique biological samples analyzed for each tissue, we first evaluated the variability of adduct ratios on a sample-to-sample basis. The consistency of these adduct ratios was assessed using the median of the relative standard deviation (% RSD) values of all annotated DAG species across all samples per tissue type. In a few cases, a large variance was found for adduct ratios, as exemplified for MS1 spectra of plasma DAG 36:4 with $[M + NH_4]^+$ at 634.54 *m*/*z*, $[M + Na]^+$ at 639.50 *m*/*z*, and $[M + K]^+$ at 655.47 *m*/*z* (Figure 1). These examples represent the potential for significant variation as impacted by changes in instrument conditions over time or by variations in endogenous concentrations. Yet, the median% RSD of adduct ratios across biological samples was consistently <15% RSD for the two major adduct forms (Table 1). Conversely, liver and brain samples showed higher variability for $[M + NH_4]^+$ adducts, which were consistently measured with less than 20% of the total ion abundance (Tables 1 and S1). This trend was also observed for other low-abundance adducts such as potassiated adducts and water loss ion species (Table 1). There were negligible trends observed when the samples were organized by run order (Figure S1).

While each DAG was robustly measured at <15% RSD for the dominant $[M + NH_4]^+$ and $[M + Na]^+$ adducts across samples for each matrix type, we found profound differences in the total adduct ratios between the DAG species observed within these matrices. For example, on average $[M + NH_4]^+$ ions made up 32% of the total intensity of all of the adducts across the 15 DAG species in plasma (Table 2). Yet, some DAGs showed 13% abundance for $[M + NH_4]^+$, while other DAGs were present at 77% abundance (Figure 2, Table S1). Hence, the variance of ion ratios across the different DAG species was

markedly higher than the measurement variance across samples. We found considerably lower variance of adduct ratios for DAG species in gonadal and inguinal fat compared to other matrix types.

However, significant changes in these ratios were still observed between specific annotations within fat tissues. For example, DAG 30:0 was detected with 62% abundance for the $[M + Na]^+$ adduct and 23% for the $[M + NH_4]^+$ adduct in inguinal fat. Conversely, DAG 36:3 was present at a 35% relative ratio for the $[M + Na]^+$ adduct and 55% for the $[M + NH_4]^+$ adduct. Therefore, even among the lesser variability of adipose tissue, we found up to 30% difference in adduct ratios between DAG species. This finding contradicts the notion that a single ion adduct might suffice to universally quantify lipids across an entire lipid subclass in any specific matrix type.

Variance of adduct ratios was even greater between matrix types (Figure 2A, Tables 2 and S1). Overall, sodiated adducts were detected at consistently high ratios across all matrices. For low abundant DAG species, sometimes the sodiated adducts were the only detectable ion species, whereas for other DAG species, the sodiated adducts could form less than 10% of the total ion abundance (Figure 2A, Table S1). Similarly, the abundance of ammoniated adducts ranged from 90% to less than 5% for different DAG species across all matrices. Again, this finding reinforces the idea that a single adduct ion is not as reliable in the application of relative quantification methods or estimations of total lipid concentrations in classes that form multiple abundant adducts, such as DAGs. In some tissues, potassiated and neutral loss ion species reached up to 20% of the overall DAG ratio for individual DAG lipids (Figure 2A, Table S1). For example, the water neutral loss ion for DAG 34:1 reached 33% abundance in brain tissues, while DAG 38:5 was detected at 23% abundance for the $[M + K]^+$ adduct in plasma (Figure 2B). DAG 36:3 showed up to 70% ion ratios for ammoniated adducts for fat and muscle tissues but considerably lower abundance in other matrices with only 15% abundance in liver (Figure 2B, Table S1). Overall $[M + H - H_2O]^+$ adduct ratios were noticeably higher in liver, kidney, heart, and brain (Figure 2a), specifically for DAG 34:1 and DAG 36:3 but nearly absent in other matrices while water loss adduct ions in DAG 38:5 were consistently low abundant even in liver, kidney, heart, and brain (Figure 2b). Hence, ion ratios were found to be impacted by both the matrix-specific batches and the ionization patterns of individual DAG species.

Factors Contributing to Variance in Adduct Ratios.

The observed variance between compounds in adduct formation for DAG lipids led us to examine DAG-specific properties that might impact the variation of adduct ratios. Here, we focused on three possible factors influencing adduct ratios: (a) carbon chain lengths, (b) degree of fatty acyl unsaturation, and (c) the absolute peak intensity of DAG species (Figure 3). We saw a remarkably consistent trend in decreasing abundance for $[M + Na]^+$ ions in plasma with increasing carbon chain lengths from 32 to 40 total carbons (Figure 3A, right panel). This decrease was balanced by an increase in the formation of ammoniated adduct ions, while the ratio of potassiated adducts remained stable with increasing acyl chain lengths (Figure 3). We summarized these observations for all DAG species and across all eight matrices in a heat map, showing that ammoniated adducts were consistently increased

in abundance with an increasing number of carbons across all tissues (Figure 3A, left panel). However, sodiated and ammoniated trends were not always opposite. For example, brain DAG species represented the largest trend differences for $[M + NH_4]^+$ ions with a 30% ratio increase from 32 to 40 total carbons. Yet, sodiated DAG species in brain tissues remained fairly stable, while potassiated and water loss ion ratios both showed a consistent decrease with increased carbon chain lengths. In kidney, decreases in water loss ion ratios were also found with larger carbon chain lengths, whereas other matrix types showed only modest or no trends in adduct ratios, with the exception of ammoniated ions.

Overall, very similar trend patterns were found for an increasing number of double bonds (Figure 3B). Again, the largest differences were found for plasma, specifically for the sodiated and ammoniated adducts (Figure 3B). Potassiated adducts showed minimal changes across all tissues, while water loss ion ratios consistently decreased with higher levels of unsaturation for all matrix types for which these ions were detectable. Interestingly, a 15% increase in the adduct ratio for sodiated adducts was observed in brain tissue. Taken together, these observations detail strong structural influences on adduct formation in DAG species that is correlated to both carbon chain length and degree of unsaturation, especially for primary adduct forms.[25] To address a potential bias in the analysis due to the correlation of carbon chain lengths and degree of unsaturation, we repeated the analyses across increasing numbers of double bonds in C34 and C36 DAGs, as well as across monounsaturated and diunsaturated species of increasing carbon chain length (Figure S2). The same overall trends were observed as before, indicating that both parameters contributed to differences in ion ratios.

Last, we assessed absolute peak intensity as an independent factor. The few DAG species measured with 100% $[M + Na]^+$ across the different data sets were relatively low abundant, suggesting a connection between the biological concentration and adduct formation. Overall, only very modest trends were observed with high variance across intensity values and adduct species. For example, in plasma only very slight decreases were found for sodiated and ammoniated adducts (Figure 3C, right panel) and even absent trends in other tissues such as heart muscle. Nonetheless, sodiated adducts decreased with increased peak intensity in inguinal fat, gastrocnemius muscle, and kidney tissues at −10% levels. Other matrices showed less than 10% change in either direction, except for brain tissues, which showed a 19% decrease in $[M + NH_4]^+$ and a 16% increase in $[M + K]^+$ in correspondence to increased peak intensities. Overall, therefore, trends in adduct formation was mostly impacted by carbon chain lengths and degree of unsaturation but not by total peak intensities. Yet, the complexity of these processes inhibits accurate predictions regarding adduct formation in different matrix types or instrument conditions.

Other factors that we did not systematically evaluate were variance between instruments, reproducibility of buffer compositions across batches, or the stability of instrument conditions over time. Indeed, instrument conditions greatly affect the mechanisms of adduct formation[11,26] as well as in-source fragmentation.[27] In the present study, two LC-Orbitrap HF mass spectrometers were used during acquisition and led to distinct shifts in the relative adduct ratios, particularly with respect to water loss ion species. The prevalence of these water losses is likely due to different ion source conditions because other parameters such

as solvents, flow rates, and buffers were kept identical.[27] Biological influences also serve as potential instigators of matrix-specific changes in adduct formation. Similar to the trends observed for peak intensities of individual lipid species, total lipid content is also known to slightly influence instrument response and could help explain the comparable adduct trends in the lipid-rich adipose and gastrocnemius tissues.[28] Additionally, the formation of alkali metal adducts has often been linked to in vivo concentrations and may be strongly impacted by matrix effects.[29] This idea is supported by the notable differences in potassium adduct ion abundance between gonadal and inguinal fat samples. Similarly, the primary adduct for most DAGs, $[M + Na]^+$, presents average shifts of 10–15% between the different data sets acquired on the same LC–MS system, again indicating potential influence of endogenous sodium levels. It is therefore reasonable to assume that the variation observed between data sets is caused by a combination of technical and biological factors. We therefore set out to determine a more robust choice in the use of internal standards to address both types of variance.

Adduct Selection for Accurate Quantification.

While relative quantitation has remained the primary approach for nontargeted analyses, there have been increasing efforts to incorporate more robust methods for absolute quantification into these workflows.[30,31] Although detailing true absolute concentrations is unrealistic for thousands of nontargeted analytes, standardized comparisons of lipidomic analyses across batches, instruments, and laboratories must transit from reporting arbitrary peak intensities to estimates of molar concentration.[32] Current methods use single-point calibration or surrogate calibrants with appropriate correction factors to account for changes in ionization efficiencies within lipid subclasses.[33] In addition, the nonlinearity of signal responses should be considered.[34] In estimating molar concentrations using these procedures, the impact of adduct formation has been underexplored, possibly due to the assumption that isotopically labeled internal standards will behave nearly identical to their corresponding endogenous compound. While this is likely true for each identical pair of endogenous lipid species and its exact isotope-labeled counterpart, we here see that such comparisons do not hold true across all species in a lipid subclass like DAGs, even among similarly structured species. Therefore, we investigated the influence of joining adduct intensities on the accuracy of absolute quantification in comparison with utilizing a single representative adduct form.

First, to ensure that there were no unintended effects of combining adducts on data interpretation, we evaluated the median precision of absolute peak intensity measurements across 25 QC samples (Table S2). All annotated DAG species across the eight matrix types exhibited an equal or improved precision for combined adducts in comparison to measuring only a single adduct form. Thus, we infer that data quality either improves or stays the same when adducts are joined. We then evaluated quantitative accuracy for monounsaturated DAG species using different adducts and combinations of adducts. Specifically, we studied peak intensities of sodiated and ammoniated adducts in isolation, in combination between these two dominant ions, and in combination of all four adduct forms. For this evaluation, we employed three deuterated monounsaturated DAG internal standards with DAG 31:1-d5 at 25 μg/mL extraction solvent, DAG 33:1-d5 at 50 μg/mL, and DAG 35:1-d5 at 75

μg/mL. The concentrations of DAG species were adjusted to the extraction solvent volume for the different matrices and plotted against the total peak intensity for each adduct combination (Figure 4A). The three concentrations of DAG internal standards were fitted with a linear regression and the resulting slope was used for absolute quantification. All adduct combinations displayed a R^2 value greater than 0.94.

We theorized that joining all four adduct forms provided the most accurate concentrations because it encompassed all available data for the specific compound. Yet, even this estimate of quantitative concentrations may still include unrecognized systematic errors. We then compared calculated endogenous DAG concentrations for $[M + Na]^+$, $[M + NH_4]^+$, and {$[M + Na]^+$ and $[M + NH_4]^+$} against the combination of all four adducts (Figure 4B). When solely relying on $[M + Na]^+$ ions for quantification, differences of up to 25% in absolute concentrations were found compared to the use of all four adducts across the eight data sets, as exemplified in measuring DAG 34:1 in gastroc tissues. Overall, however, most DAG species quantified by $[M + Na]^+$ showed a difference in estimated molar concentrations of less than 10% in the different tissues. Conversely, when only $[M + NH_4]^+$ ions were used for quantifications, most DAG species showed more than 20% quantification errors (Figure 4B). Importantly, the combination of sodiated and ammoniated adduct intensities, {$[M + Na]^+$ and $[M + NH_4]^+$}, proved to be the most reliable way to measure DAG concentrations with only a maximum of 5% difference to the calculated concentrations from using all adducts (including potassiated and water loss ion species). We therefore strongly recommend using the most dominant ion species in lipid quantifications, especially for DAGs, to correct adduct formation differences among matrix types. Interestingly, we found that the presumed accuracy of quantifying endogenous DAG lipid using a single adduct was correlated to the respective adduct ratios between the internal standard and the endogenous lipid species. Figure 5 demonstrates that when the response ratio of a single adduct varied by >20% between the endogenous species and the corresponding internal standard, the absolute concentration would also vary by >20% with respect to our control of using all four adduct forms.

CONCLUSIONS

From these observations, we suggest that the relative ratio of adducts is the most important variable to consider for quantitative accuracy. To avoid significant inaccuracies in the relative and absolute ends of quantification, at least 80% of the total abundance should be contained within the adducts selected for analysis. Nontargeted lipidomic studies performed across multiple batches, different LC–MS systems, or separate laboratories should prioritize the proper adduct selection to ensure sufficient data transferability for quantitative analyses.

Supplementary Material

Refer to Web version on PubMed Central for supplementary material.

ACKNOWLEDGMENTS

The authors would like to thank Nathanial Chase Stevens, Zachary Rabow, and Sara Greenfield for their assistance with the sample preparation and mass spectrometry analyses. We would also like to thank Richard A. Miller at the

University of Michigan for providing the mouse tissue samples as part of the NIH Longevity Consortium (LC). This study was supported by the National Institutes of Health grants U19 AG023122 and R01HL157535.

REFERENCES

(1). Olshansky G; Giles C; Salim A; Meikle PJ Prog. Lipid Res 2022, 87, 101177. [PubMed: 35780914]

(2). Ghorasaini M; Mohammed Y; Adamski J; Bettcher L; Bowden JA; Cabruja M; Contrepois K; Ellenberger M; Gajera B; Haid M; Hornburg D; Hunter C; Jones CM; Klein T; Mayboroda O; Mirzaian M; Moaddel R; Ferrucci L; Lovett J; Nazir K; Pearson M; Ubhi BK; Raftery D; Riols F; Sayers R; Sijbrands EJG; Snyder MP; Su B; Velagapudi V; Williams KJ; de Rijke YB; Giera M Anal. Chem 2021, 93, 16369–16378. [PubMed: 34859676]

(3). Triebl A; Burla B; Selvalatchmanan J; Oh J; Tan SH; Chan MY; Mellet NA; Meikle PJ; Torta F; Wenk MR J. Lipid Res 2020, 61, 105–115. [PubMed: 31732502]

(4). Ulmer CZ; Koelmel JP; Jones CM; Garrett TJ; Aristizabal-Henao JJ; Vesper HW; Bowden JA Lipids 2021, 56, 3–16. [PubMed: 32519378]

(5). Cajka T; Fiehn O Anal. Chem 2016, 88, 524–545. [PubMed: 26637011]

(6). Khan MJ; Codreanu SG; Goyal S; Wages PA; Gorti SKK; Pearson MJ; Uribe I; Sherrod SD; McLean JA; Porter NA; Robinson RAS Rapid Commun. Mass Spectrom 2020, 34, No. e8911.

(7). Mortier KA; Zhang G; Van Peteghem CH; Lambert WE J. Am. Soc. Mass Spectrom 2004, 15, 585–592. [PubMed: 15047063]

(8). Murphy RC TrAC, Trends Anal. Chem 2018, 107, 91–98.

(9). Kruve A; Kaupmees KJ Am. Soc. Mass Spectrom 2017, 28, 887–894.

(10). Knittelfelder OL; Weberhofer BP; Eichmann TO; Kohlwein SD; Rechberger GN J. Chromatogr. B 2014, 951–952, 119–128.

(11). Alechaga E; Moyano E; Galceran MT Bioanal. Anal. Chem 2016, 408, 1269–1277.

(12). Dziadosz MJ Chromatogr. B 2018, 1084, 1–3.

(13). Yang XJ; Qu Y; Yuan Q; Wan P; Du Z; Chen D; Wong C Analyst 2013, 138, 659–665. [PubMed: 23181258]

(14). Gonzalez-Riano C; Gradillas A; Barbas CJ Chromatogr. Open 2021, 1, 100018.

(15). Abbassi-Ghadi N; Jones EA; Gomez-Romero M; Golf O; Kumar S; Huang J; Kudo H; Goldin RD; Hanna GB; Takats ZJ Am. Soc. Mass Spectrom 2016, 27, 255–264.

(16). DeFelice BC; Mehta SS; Samra S; Cajka T; Wancewicz B; Fahrmann JF; Fiehn O Anal. Chem 2017, 89, 3250–3255. [PubMed: 28225594]

(17). Kuhl C; Tautenhahn R; Böttcher C; Larson TR; Neumann S Anal. Chem 2012, 84, 283–289. [PubMed: 22111785]

(18). Broeckling CD; Afsar FA; Neumann S; Ben-Hur A; Prenni JE Anal. Chem 2014, 86 (14), 6812–6817. [PubMed: 24927477]

(19). Kachman M; Habra H; Duren W; Wigginton J; Sajjakulnukit P; Michailidis G; Burant C; Karnovsky A Bioinformatics 2020, 36, 1801–1806. [PubMed: 31642507]

(20). Miller RA; Harrison DE; Astle CM; Fernandez E; Flurkey K; Han M; Javors MA; Li X; Nadon NL; Nelson JF; Pletcher S; Salmon AB; Sharp ZD; Van Roekel S; Winkleman L; Strong R Aging Cell 2014, 13, 468–477. [PubMed: 24341993]

(21). Koelmel JP; Kroeger NM; Gill EL; Ulmer CZ; Bowden JA; Patterson RE; Yost RA; Garrett TJ J. Am. Soc. Mass Spectrom 2017, 28, 908–917. [PubMed: 28265968]

(22). Tsugawa H; Cajka T; Kind T; Ma Y; Higgins B; Ikeda K; Kanazawa M; VanderGheynst J; Fiehn O; Arita M Nat. Methods 2015, 12, 523–526. [PubMed: 25938372]

(23). Kind T; Liu K; Lee DY; DeFelice B; Meissen JK; Fiehn O Nat. Methods 2013, 10, 755–758. [PubMed: 23817071]

(24). Fan S; Kind T; Cajka T; Hazen SL; Tang WHW; Kaddurah-Daouk R; Irvin MR; Arnett DK; Barupal DK; Fiehn O Anal. Chem 2019, 91, 3590–3596. [PubMed: 30758187]

(25). Broeckling CD; Ganna A; Layer M; Brown K; Sutton B; Ingelsson E; Peers G; Prenni JE Anal. Chem 2016, 88 (18), 9226–9234. [PubMed: 27560453]

(26). Li X; Ma M; Scherban K; Tam YK Analyst 2002, 127, 641–646. [PubMed: 12081042]
(27). Criscuolo A; Zeller M; Fedorova MJ Am. Soc. Mass Spectrom 2020, 31, 463–466.
(28). Koivusalo M; Haimi P; Heikinheimo L; Kostiainen R; Somerharju PJ Lipid Res. 2001, 42, 663–672.
(29). Erngren I; Haglof J; Engskog MKR; Nestor M; Hedeland M; Arvidsson T; Pettersson CJ Chromatogr. A 2019, 1600, 174–182.
(30). Wang M; Wang C; Han X Mass Spectrom. Rev 2017, 36, 693–714. [PubMed: 26773411]
(31). Rakusanova S; Fiehn O; Cajka T TrAC, Trends Anal. Chem 2023, 158, 116825.
(32). Lange M; Fedorova M Anal. Bioanal. Chem 2020, 412, 3573–3584. [PubMed: 32240327]
(33). Drotleff B; Illison J; Schlotterbeck J; Lukowski R; Lämmerhofer M Anal. Chim. Acta 2019, 1086, 90–102. [PubMed: 31561798]
(34). Yu H; Huan T Anal. Chem 2021, 93 (4), 2254–2262. [PubMed: 33400486]

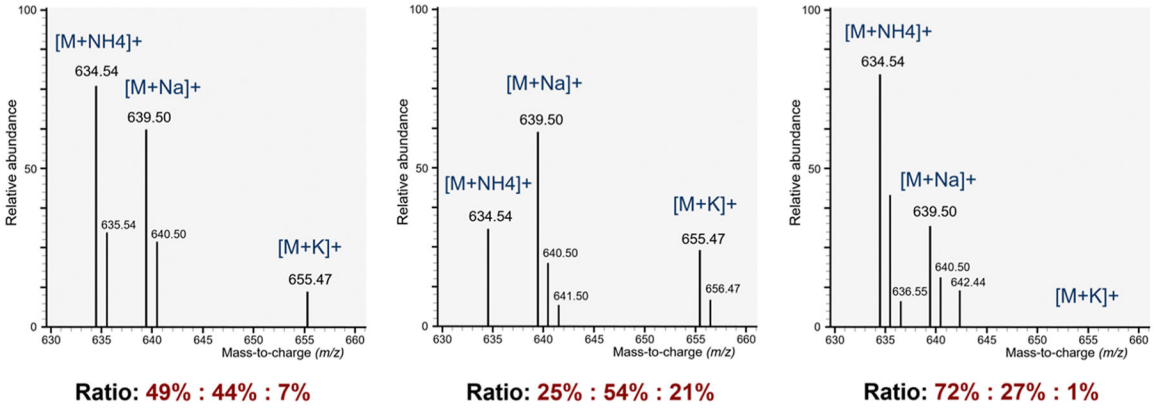

Figure 1.

Examples of measurement variance in ratios of $[M + NH_4]^+$, $[M + Na]^+$, and $[M + K]^+$ ion types for an endogenous diacylglyceride, DAG (36:4), between three individual mouse plasma samples across one batch of lipidomics LC–HRMS analyses.

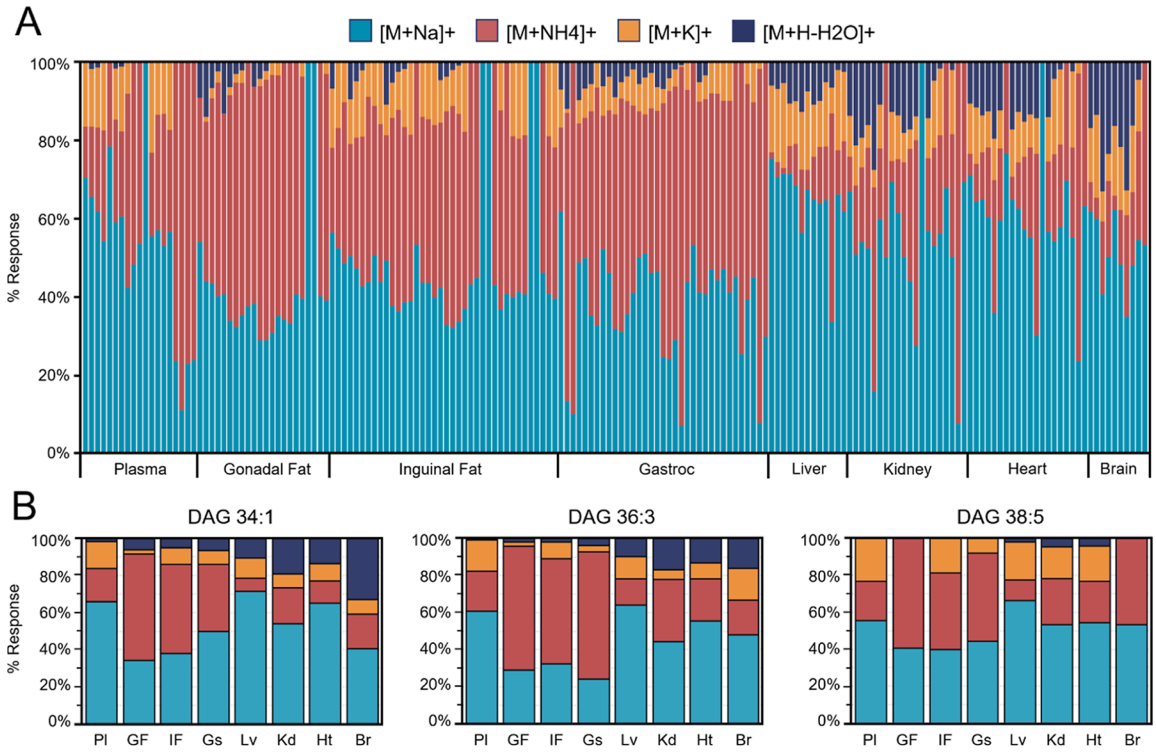

Figure 2.

(A) Graphical representation of response ratios of all annotated endogenous DAG species for $[M + Na]^+$, $[M + NH_4]^+$, $[M + K]^+$, and $[M + H - H_2O]^+$ adducts in pooled QC samples across the eight mouse matrices analyzed. (B) Average adduct ratios for each matrix type between three commonly found DAG species.

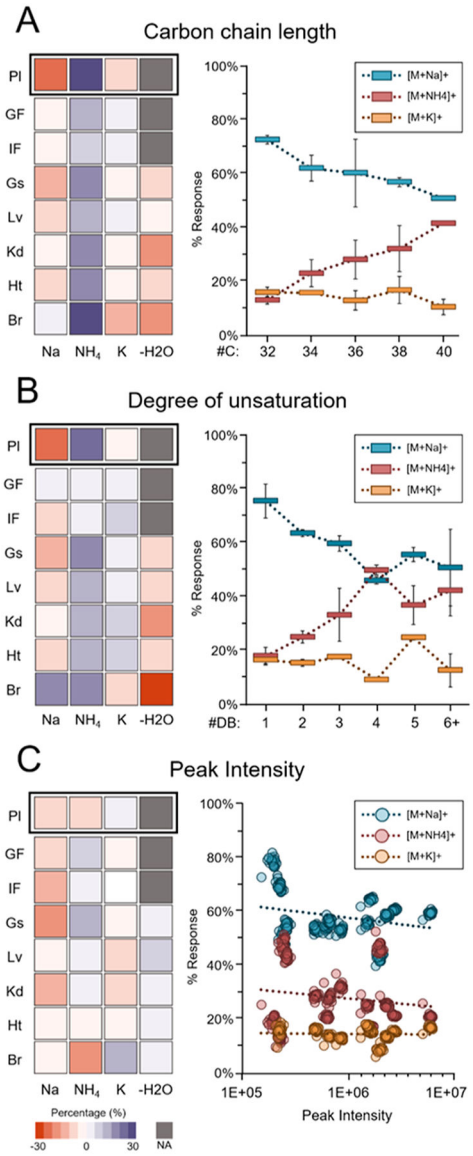

Figure 3.

Changes in average adduct ratios across pooled QC samples. Left panels: heat maps per organ (blue: highest, red: lowest; gray: sporadic or no detection) Pl, plasma; GF, gonadal fat; IF, inguinal fat; Gs, gastrocnemius muscle; Lv, liver; Kd, kidney; Ht, heart, and Br, brain. Right panels: trend graphs averaging all organs. (A) Relative abundance per number of carbons. (B) Relative abundance per number of double bonds. (C) Relative abundance per average peak intensity across pooled QC samples.

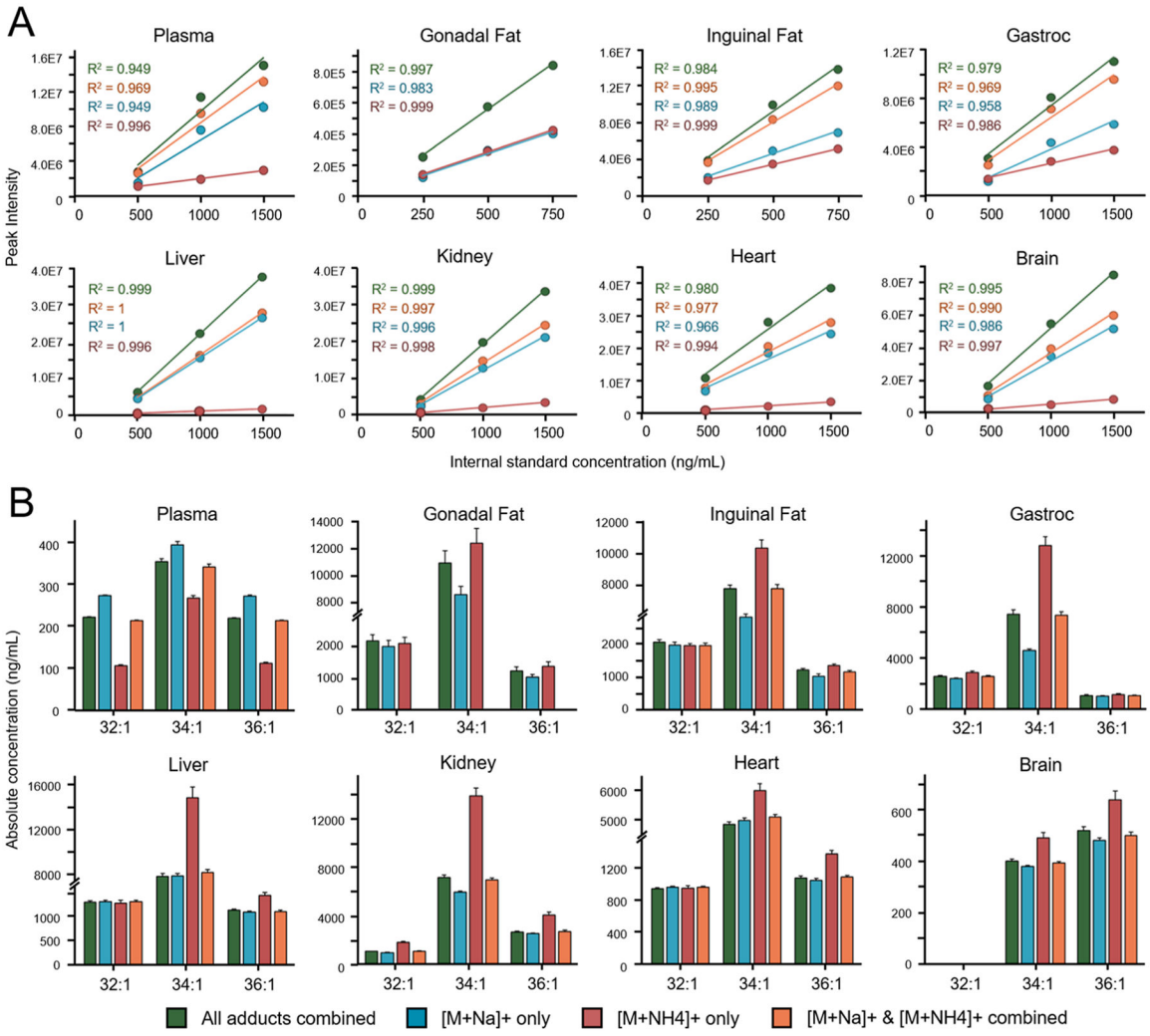

Figure 4.

(A) Linearity of three deuterated, monounsaturated DAG internal standards through different combinations of adduct ions. (B) Estimated molar concentrations of DAG 32:1, DAG 34:1, and DAG 36:1 were calculated from the slopes of the deuterated standard peak intensities. The same combinations of adducts were used between the standards and endogenous DAG compounds.

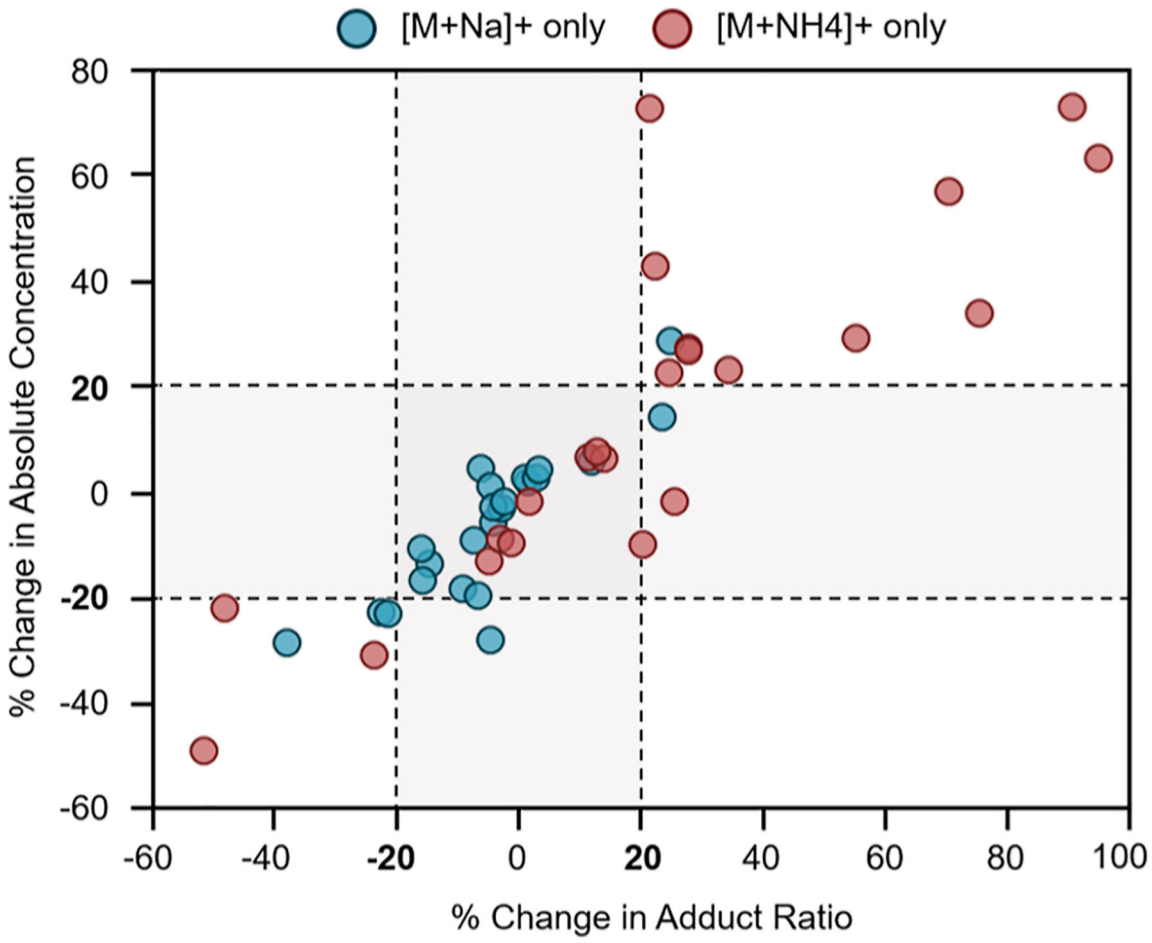

Figure 5.
Correlation of the percent change in absolute concentrations and percent change in adduct ratios between endogenous DAGs and the corresponding deuterated DAG standards.

Table 1.

Overall Measurement Variance (Median % RSD) of the Ratio of Adduct Forms in Diacylglycerides across Biological Samples

matrix type	number of samples	$[M + Na]^+$ (%)	$[M + NH_4]^+$ (%)	$[M + K]^+$ (%)	$[M + H - H_2O]^+$ (%)
plasma	279	6.9	17.7	19.1	
gonadal fat	277	9.4	6.3	19.3	
inguinal fat	279	7.5	7.8	13.5	
gastroc	245	7.4	10.1	17.3	51.4
liver	275	5.6	25.0	22.7	37.4
kidney	265	5.9	15.2	21.5	14.8
heart	268	3.5	18.0	22.1	18.0
brain	278	13.4	20.2	31.6	23.3

Table 2.

Average Adduct Ion Ratios (±SD) across All Measured DAG Species for Each Matrix Type

matrix type	number of DAG species	$[M + Na]^+$ (%)	$[M + NH_4]^+$ (%)	$[M + K]^+$ (%)	$[M + H - H_2O]^+$ (%)
plasma	15	57 ± 12	32 ± 11	15 ± 4	
gonadal fat	20	38 ± 6	57 ± 9		
inguinal fat	34	43 ± 6	44 ± 9	14 ± 4	
gastroc	34	40 ± 14	51 ± 17	8 ± 2	
liver	13	69 ± 9	12 ± 4	16 ± 4	8 ± 3
kidney	18	49 ± 16	31 ± 20	11 ± 4	17 ± 4
heart	18	57 ± 14	22 ± 15	13 ± 4	13 ± 3
brain	10	53 ± 9	19 ± 10	14 ± 5	21 ± 7